

# Flow-Induced Flutter of a Hanging Banner: A Configuration for Validation of Computational Models

Zhongwang Dou<sup>1</sup>, Aaron Rips<sup>2</sup>, Lauren Jacob<sup>3</sup>, Nathaniel Welsh<sup>3</sup>, Jung-Hee Seo<sup>4</sup> and Rajat Mittal<sup>5†</sup>  
*Johns Hopkins University, Baltimore, MD, 21218*

**Flow-induced flutter of elastic membranes presents interesting flow-structure interaction physics. Recent advances in computational modeling and computing power are enabling simulation of such problems in unprecedented detail. However, appropriate experiment that would allow comprehensive validation of such models is lacking. To fill this gap, we conduct experiments on flow-induced flutter of a hanging banner in a low Reynolds number wind tunnel using a high-speed imaging. Silicon sheets of two different thicknesses are used as the membrane material for the hanging banner and the other variables in the study are the flow speed and the banner yaw angle. A variety of flutter regimes are observed for the parameters studied here and sufficient data is provided to enable the computational modeling of this configuration.**

## I. Nomenclature

$l, w, t$	=	Membrane length, width, and thickness
$U$	=	Wind tunnel inlet flow velocity
$\rho_b, \rho_f$	=	Density of membrane, density of air
$m$	=	Mass of membrane
$\nu$	=	Air kinematic viscosity
$g$	=	Gravitational constant
$E$	=	Young's modulus
$I$	=	Second moment of area
$\theta_Y$	=	Yaw angle
$\Phi$	=	Banner deflection angle
$\Phi_{\text{mean}}$	=	Mean of banner deflection angle
$\Phi_{\text{RMS}}$	=	Root mean square of banner deflection angle
$f_\Phi$	=	Banner flutter frequency

## II. Introduction

Flow-induced flutter (FIF) has become a topic of significant interest. FIF features in a variety of engineering applications including aircraft wings and control surfaces[1], helicopter rotors, biological and bioinspired locomotion in fluid (swimming and flying)[2, 3], physiological flows (such as heart valves and vocal fold vibration)[4], heat transfer enhancement [5], and piezo electric energy harvesting[6], just to name a few. Furthermore, highly flexible bodies such as thin membranes present rich, coupled dynamics which not only serve as configurations for the study of nonlinear dynamical phenomena, they also pose significant challenges for CFD modeling and simulation. Over the past decade a number of fluid structure interaction (FSI) simulation techniques have been developed to model these complex multiphysics systems[7]. However, while the FSI community has progressed to increasingly complex FIF

---

<sup>1</sup> Postdoctoral Fellow, Department of Mechanical Engineering

<sup>2</sup> Ph.D. Student, Department of Mechanical Engineering

<sup>3</sup> Undergraduate Student, Department of Mechanical Engineering

<sup>4</sup> Associate Research Professor, Department of Mechanical Engineering

<sup>5</sup> Professor, Department of Mechanical Engineering Department. Associate Fellow AIAA

† Corresponding to: [mittal@jhu.edu](mailto:mittal@jhu.edu)

configurations, there continues to exist, a largely unmet need for experiments that can be employed for comprehensive validation of these computational model.

While experimental investigations of FIF abound, particularly in the arena of flag and filament flutter [8-13], few if any of these experiments are well suited for quantitative validation of computational models. Consequently, computation modeling of FIF within the CFD community has proceeded mostly without the benefit of such validation. From the perspective of CFD validation, the following are the desirable features of a FIF validation experiment:

- a) The configuration should be "canonical," i.e. relatively simple, with a limited set of parameters, and yet, capable of exhibiting a wide range of physical phenomena.
- b) The FIF phenomena should occur over a broad range of Reynolds numbers, ranging from low  $O(100)$  to  $>O(10^5)$  so as to allow validation of DNS, LES and RANS methodologies.
- c) The configuration should generate considerable three-dimensional effects, yet be reducible to a nominally two-dimensional configuration to enable the deployment of "cheap" 2D simulations.
- d) The material properties of the fluttering element, and the boundary conditions for the flow as well as the fluttering element, should be defined and cataloged in a precise manner.
- e) Experiments should measure a sufficient set of quantities associated with both the fluttering element (frequency, mode shapes, etc.) as well as the flow so as to enable comprehensive validation.

Guided by the above principles, we propose the configuration of a rectangular deformable membrane suspended from a horizontal support, i.e. a "hanging banner," in a parallel, uniform flow ( $U$ ) with adjustable yaw angle ( $\theta_y$ ). In addition to the material parameters of the membrane, the other key parameters are the Reynolds number, the yaw angle of the membrane and the membrane aspect-ratio. We have studied this problem experimentally in a low Reynolds number wind tunnel where it exhibits a wide variety of 2D as well as 3D flutter dynamics that are quite sensitive to flow velocity. Preliminary FIF simulations of this configuration using an immersed boundary solver are also presented.

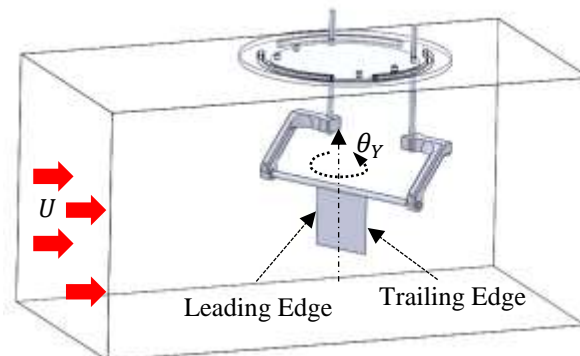


**Fig. 1 Schematic of hanging banner configuration.**

### **III. Experiment Configuration**

#### **A. Experimental Setup**

The experiment is conducted in a customized open-loop low Reynolds number wind tunnel shown in Fig. 2(a). The wind tunnel system consists of an inlet with a contraction, a (12"x 12" x 24") test section, an expansion with a fan. The fan (Cincinnati Fan 18-6-35), is driven by a three-phase 0.75hp AC motor (Baldor M3542). It is mounted at the outlet to drive the air flow, producing maximum flow volume rate of 4000 CFM. An AC motor frequency driver (VFD, ABB ACS150) is employed to vary the flow speed in the test section directly. Flow straighteners in the inlet of the contraction (honeycomb with diameter of 0.5"), as well as the inlet and outlet of the test section (honeycomb with diameter of 0.125"), are employed to obtain a uniform flow in the test section as well as to reduce the turbulence intensity in the test section. The flow inside the test section is characterized using a hot-wire anemometer (Testo 301) and found to be quite homogeneous within the test section. The measured air speed range in the test section is 0.1 – 18.4 m/s, and the turbulence intensity is measured to be below 1%.

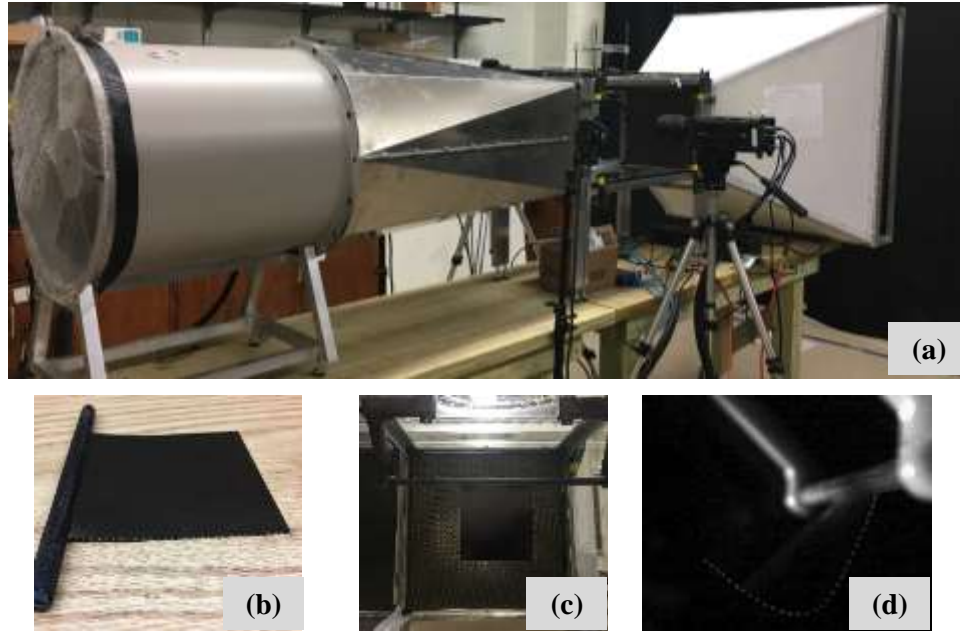


**Fig. 2. Experimental setup. (a) The low Reynolds number wind tunnel; (b) silicon sheet sample, painted black with yellow markers on the edge; (c) hanging banner inside the wind tunnel; and (d) snapshot of hanging banner fluttering in the wind tunnel.**

Silicon sheets with two different thicknesses ( $t = 0.62, 0.79$  mm) are employed as the membrane material of the hanging banner. The square banners, clamped by a cylindrical holder (0.25" diameter), have a length ( $l$ ) and width ( $w$ ) of 3" x 3" and the edges of banner are marked with an array of 31 evenly distributed yellow dots to enhance the visibility of membrane motion (Fig. 2(b) and (d)). As shown in Fig. 2(c), a mounting system is designed to hold the membrane vertically at the center of the wind tunnel test section with the yaw-angle ( $\theta_{YA}$ ) that can be adjusted from 0 (banner normal to flow) to 90 degrees (parallel to the flow).

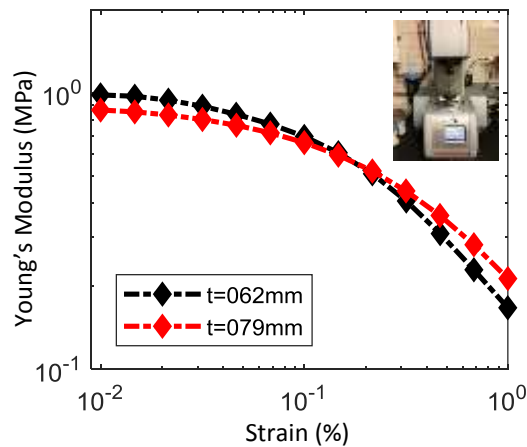


**Fig. 3. Young's Modulus for the membrane for varying strain amplitudes.**

Both silicon sheets have a density of  $\rho_b = 1.18 \times 10^3 \text{ kg/m}^3$  and the material property of silicon sheets is characterized using a rheometer (Anton-Paar Inc., MCR 302). By sweeping the amplitude of the applied strain on the rheometer at a frequency of 5 rad/s, the loss and storage Modulus of the silicon sheet is returned. Finally, by using the specified Poisson's ratio of 0.48 for these sheets, the Young's modulus is calculated (Fig. 3). We also performed a frequency sweep from 0.01 – 100 rad/s at a strain amplitude of 5% and found that the modulus varied by less than modulus 2%.

## B. Experimental conditions

Table 1 describes the test conditions in the current study. At  $\theta_Y = 0^\circ$ , only one side of the edge is currently recorded since the motion is quite two-dimensional. For  $\theta_Y = 45^\circ$ , both the leading and trailing edges are recorded. The Reynolds numbers for the cases vary from about 3,400 to 128,000. While these are higher than what is easily accessible via high-fidelity computational models, the flutter dynamics of such membranes are often insensitive to Reynolds number beyond  $O(1000)$ . Thus computational models could employ lower Reynolds numbers and still recover the observed dynamics of the membranes.

**Table 1. List of test condition.**

Membrane Thickness (mm)	Yaw angle (degree)	Velocity (m/s)
0.62	0	0.5, 1.3, 2.2, 3.1, 4.2, 5.6, 5.7, 5.8, 7.0, 8.7, 10.2, 12.1, 13.7, 15.3, 16.9
0.62	45	0.5, 1.3, 2.2, 3.1, 4.2, 5.6, 7.0, 7.5, 7.7, 7.9, 8.2, 9.4, 10.2
0.79	0	0.5, 1.3, 2.2, 3.1, 4.2, 5.6, 6.0, 6.1, 7.0, 8.7, 10.2, 12.1, 13.7, 15.3, 16.9
0.79	45	0.5, 1.3, 2.2, 3.1, 4.2, 5.6, 7.0, 7.2, 7.4, 7.7, 7.9, 8.2, 9.4, 10.2

## C. Imaging and Data Analysis

A high-speed CMOS camera (IDT Y4-S1,  $1016 \times 1016$  pixels,  $12 \mu\text{m}/\text{pixel}$ ) is employed to record the motion of membrane (Fig. 4a) under the illumination of a 250w halogen lamp. As mentioned above, each banner is coated black and 31 yellow dots on the banner edge are used for detecting the movement of the banner. The markers on the edge of the banner are identified and tracked using an in-house 4-frame particle tracking algorithm [14], as shown in Fig. 4(c) and the motion of the banner reconstructed as demonstrated in Fig. 4(d). At low flow speed, the banner exhibits no significant flutter, and we record the banner motion at 200 frames per second (fps) for 2 seconds. Once flutter occurs, the banner motion is recorded at 3000 fps for 2 seconds. The uncertainty of dot location measurement result is quantified below 5% estimated using Eq. (7.50) in Adrian and Westerweel [15].

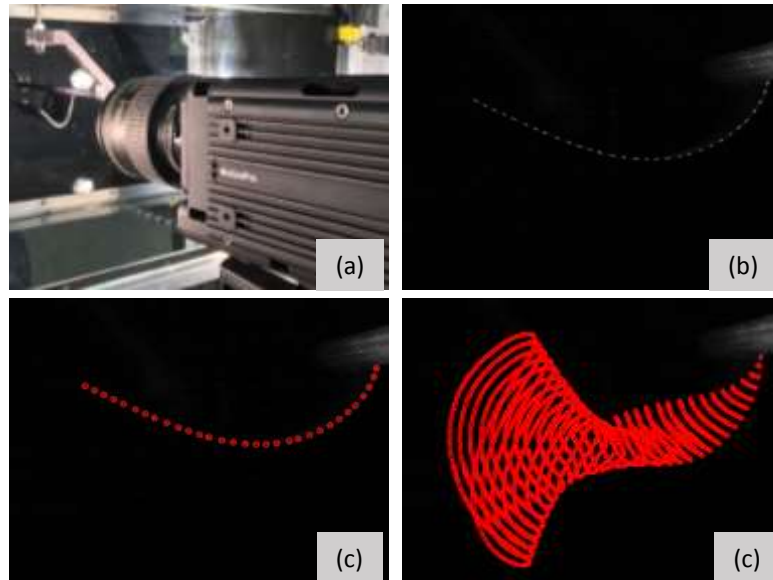


**Fig. 4. Data and imaging for 0.62mm thickness banner at flow speed of 5.8 m/s. (a) Videos are recorded using a high-speed camera; (b) snapshot of banner flutter from high-speed camera, emphasized by yellow dots along banner edge; (c) reconstruction of banner edge shape through the recognition of the yellow markers; (d) flutter pattern over time.**

To quantitatively describe the deflection, flutter intensity and frequency of the hanging banner, we focus currently on a single parameter –  $\Phi$ , the angle subtended by the tip of the banner from the vertical axis (see Fig. 6). This parameter is tracked over time during each experiment and the deflection of the banner, its flutter intensity and frequency are then represented by the mean ( $\Phi_{mean}$ ), root mean square (RMS,  $\Phi_{RMS}$ ), and frequency ( $f_{\Phi}$ ) of  $\Phi$ , respectively. Figure 6 shows an example of banner flutter in six snap shots based on 0.79 mm thickness banner at  $U = 6.1 \text{ m/s}$ ,  $\theta_Y = 0^\circ$  over 0.1 seconds.

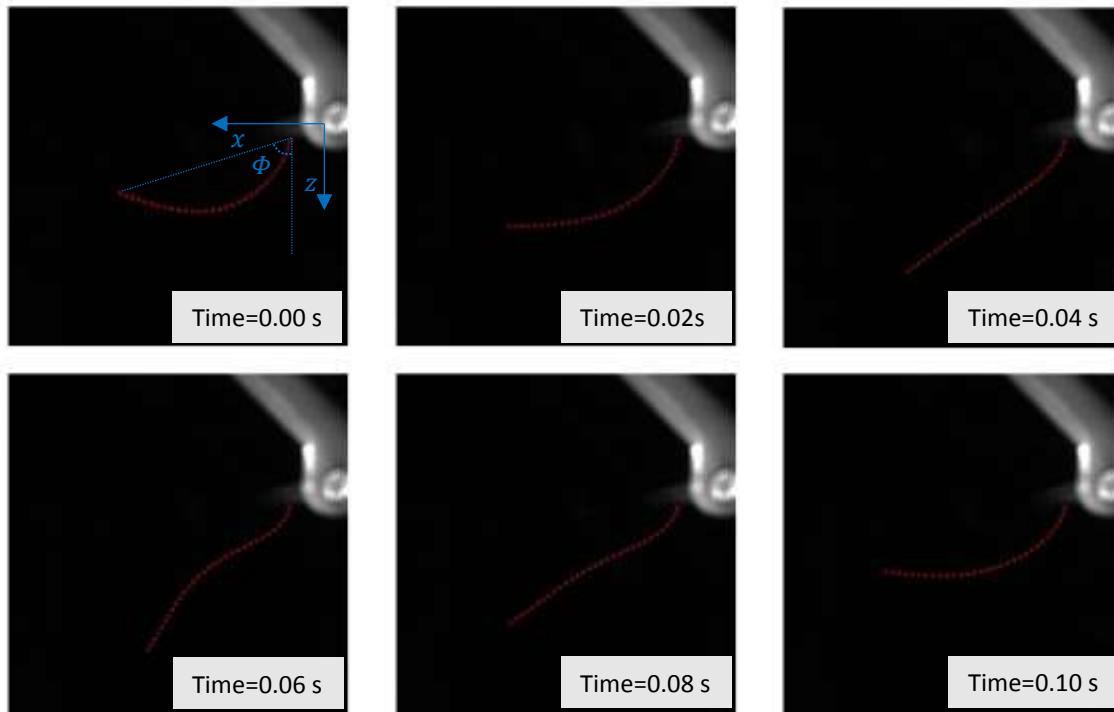


**Fig. 5. Snapshots and reconstructed banner; banner thickness=0.79 mm;  $U = 6.1 \text{ m/s}$  and  $\theta_Y = 0^\circ$ . Deflection angle  $\Phi$  is shown in the first snapshot.**

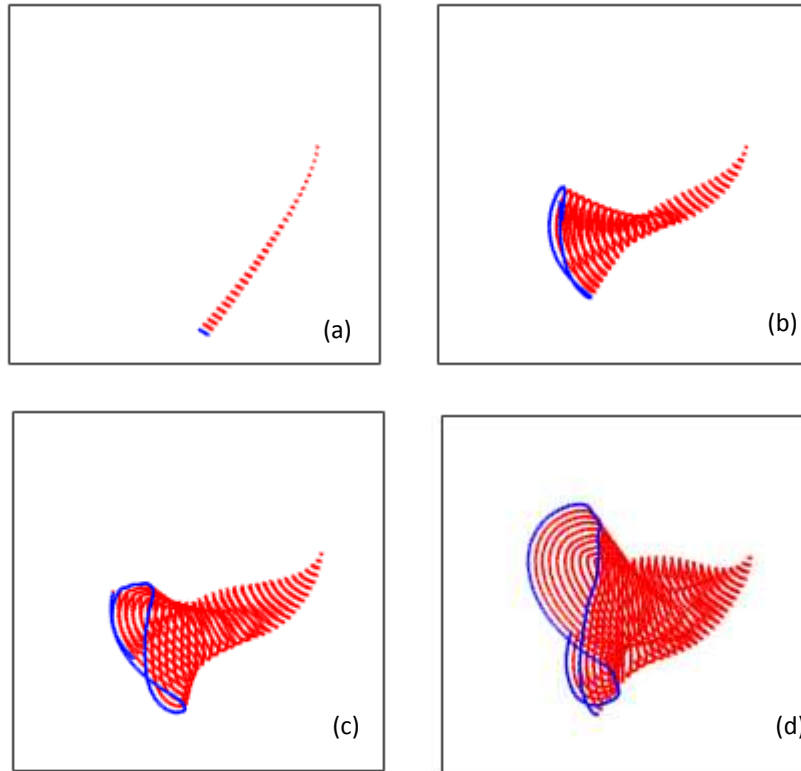
## IV. Results

### A. Banner flutter at zero yaw angle ( $\theta_Y = 0$ )

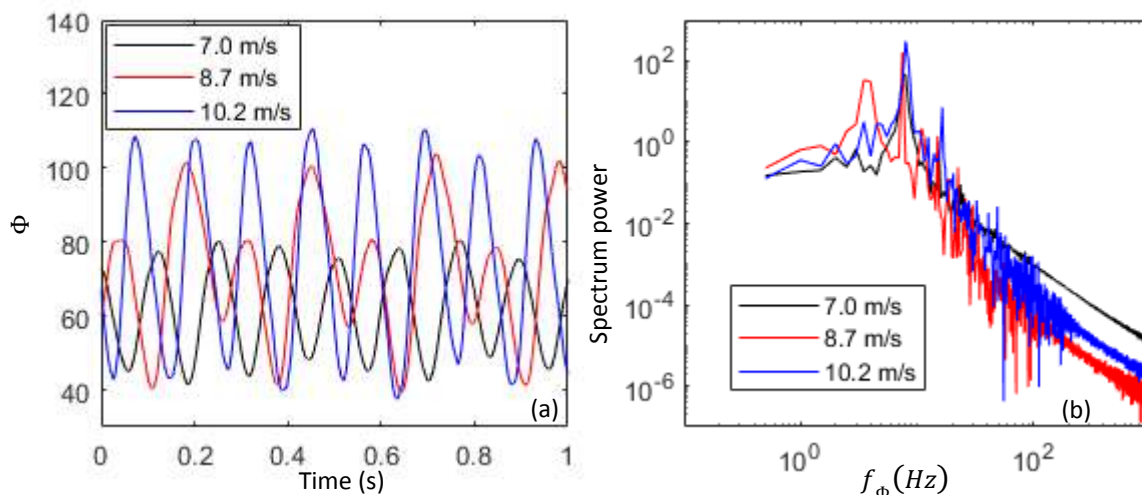
Figure 6, shows high-speed imaging data obtained for 4 selected cases that show distinct flutter phenomena. Fig. 6(a) shows the banner edge for  $U = 3.1 \text{ m/s}$  where it exhibits very small amplitude flutter whereas 6(b), which is at  $U = 7.0 \text{ m/s}$  shows noticeable and highly periodic flutter. At a higher speed of  $8.7 \text{ m/s}$ , the flutter amplitude increases and the tip of the banner exhibits a “figure 8” type of movement and this. The final plot is at a velocity of  $10.2 \text{ m/s}$  where this movement is exaggerated and the tip of the fluttering banner rises beyond the horizontal axis. Figure 7 shows the time-history of the tip-angle versus time as well as the frequency spectra for these four cases. The spectra indicate a nearly constant frequency of about 8 Hz for these cases although, for the flow velocity of  $8.7 \text{ m/s}$ , a noticeable subharmonic is also observed.

Figure 8 shows the trends in deflection, flutter amplitude and flutter frequency for all the flow speeds and a number of observations can be made from these plots. First, both banners exhibit very similar behavior although the overall deflection in the thicker membrane is slightly smaller and the flutter frequency is also slightly lower. Furthermore, for both banners, we identify four distinct regimes with increasing flow speed. The first regime extends from the lowest speed to about 6 m/s. In this regime and in this regime,  $\Phi_{mean}$  increase linearly with  $U$ , while  $\Phi_{RMS}$  stays nearly zero. This is therefore the static deflection regime. The second regime extends from a flow velocity of about 6 to 7 m/s where noticeable flutter first occurs. The distinct feature of this regime is that both  $\Phi_{mean}$  and  $\Phi_{RMS}$  increase

with velocity whereas the flutter frequency  $f_\Phi$  remains nearly constant. The third regime extends from a flow velocity of 7 to 10 m/s and in this regime,  $\Phi_{mean}$  reaches a plateau of about 70 degrees, whereas the flutter amplitude, as measured by  $\Phi_{RMS}$ , as well as the flutter frequency continue to increase nearly linearly. The fourth regime occurs for flow velocity greater than 10 m/s and in this regime, both the mean deflection and flutter amplitude are nearly constant but the flutter frequency continues to increase linearly.



**Fig. 6.** Trajectory of 0.79 mm,  $\theta_Y = 0^\circ$  banner for 4 selected flow velocities (a) 3.1 m/s, (b) 7.0 m/s, (c) 8.7 m/s (d) 10.2 m/s.



**Fig. 7.** (a) Time-history of  $\Phi$  and (b) corresponding frequency spectra for three selected cases.

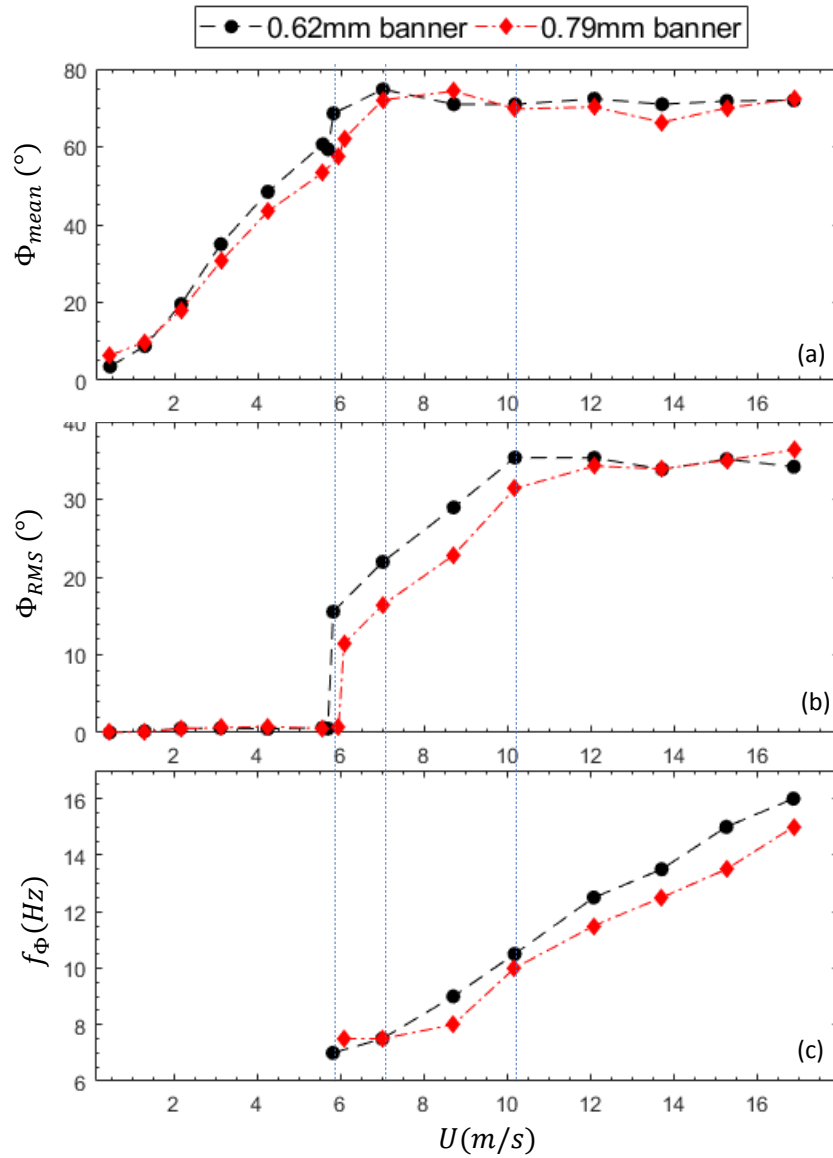
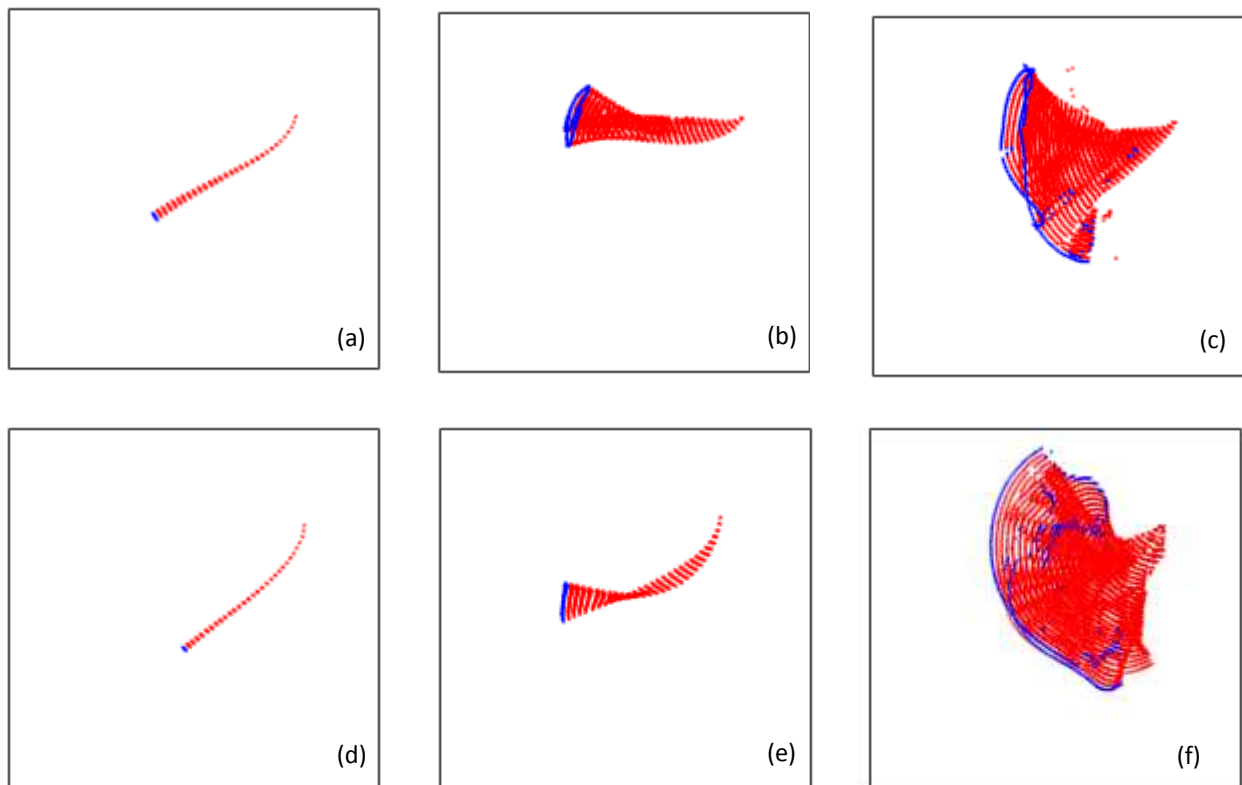


Fig. 8. Banner motion with the increase of flow velocity at  $\theta_{\gamma} = 0^{\circ}$ . (a), (b), and (c) plot the mean, RMS, frequency of  $\Phi$ , respectively, which describes the banner deflection, intensity, and frequency, respectively.

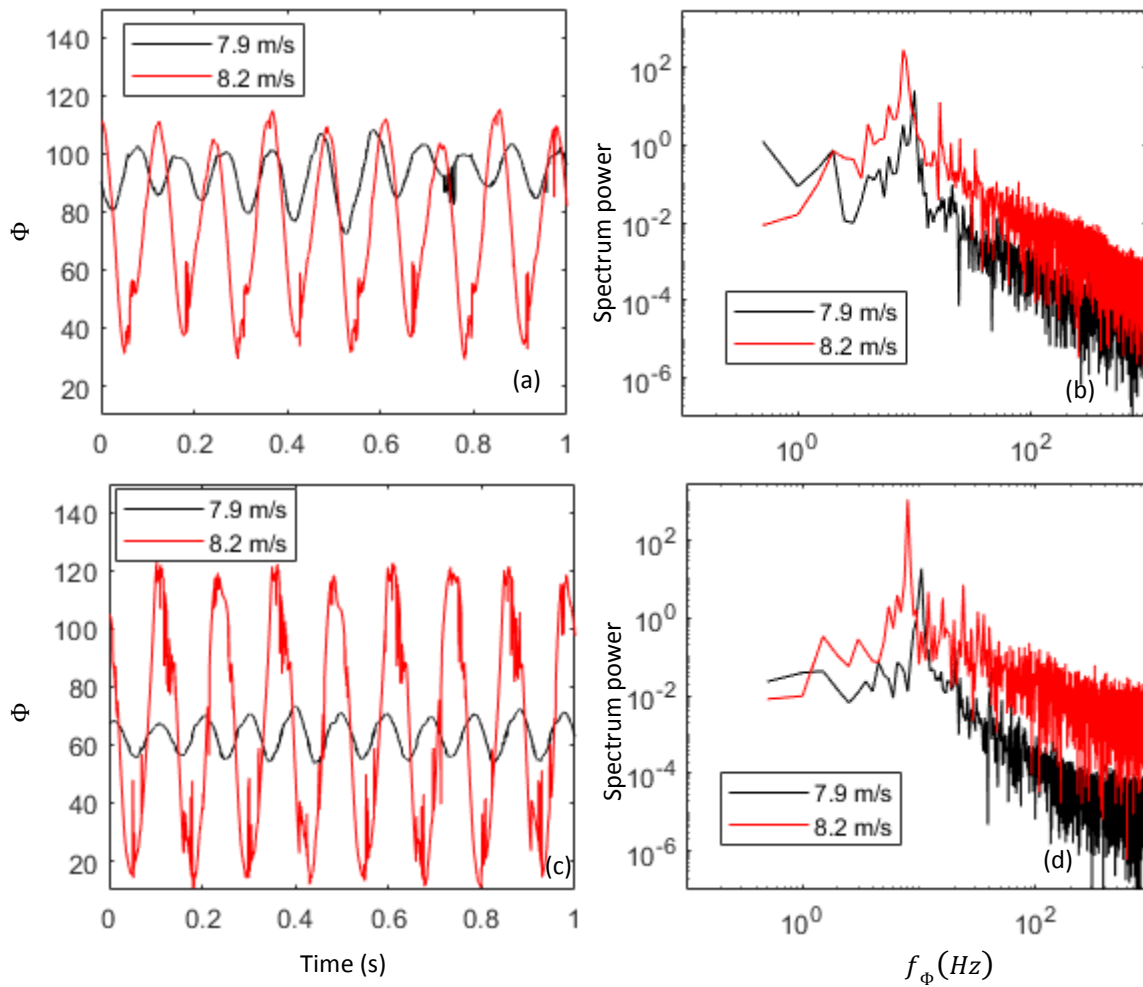
**B. Banner flutter at 45° yaw angle ( $\theta_Y = 45^\circ$ )**

Figure 9, 10, and 11 are plots for deflection and flutter of the banner with  $\theta_Y = 45^\circ$ . For this case both the leading-edge as well as the trailing edge are tracked separately. The trajectory of the banner (Fig. 9) for three selected flow velocity shows that the deflection as well as the flutter amplitude of the trailing edge is generally larger than the leading-edge. Furthermore, at the higher velocity of 8.2 m/s the trailing edge exhibits a complex motion including what may be construed as bucking and snapping.

Figure 11 shows that during the static deflection regime that extends to a velocity of about 7 m/s, the deflection of the trailing-edge is noticeably larger than the leading edge. In the narrow regime from 7-8 m/s, the banner starts to flutter with a small ( $< 8^\circ$ ) amplitude but overall there is not significant change in the deflection of the banner. Between 8 and 8.5 m/s there is a dramatic change in the dynamics of the banner, the flutter amplitude of both the leading and trailing edge increases rapidly and the mean deflection of the trailing-edge drops to become nearly equal to leading-edge. The flutter frequency is also observed to drop rapidly in this narrow regime from about 10 Hz to about 8 Hz. Beyond about 8.5 m/s, the banner enters its final regime where the mean deflection and flutter amplitude are nearly constant but the frequency increases linearly with speed.



**Fig. 9. Trajectory of banner flutter in the three regimes (blue is the tip trajectory) for 0.79 mm banner over 0.27 seconds when  $\theta_Y = 45^\circ$ . (a), (b), (c), plot the trajectory in region 1 (4.2 m/s), 2 (7.9 m/s), and 3 (8.2 m/s), respectively for the leading edge; (d), (e), (f), plot the trajectory in region 1 (4.2 m/s), 2 (7.9 m/s), and 3 (8.2 m/s), respectively for the trailing edge.**



**Fig. 10.** (a) Time-history of  $\Phi$  and (b) corresponding frequency spectra for two selected cases for the 0.79 mm  $\theta_Y = 45^\circ$  banner. (a) and (b) leading edge; (c) and (d) are trailing edge.

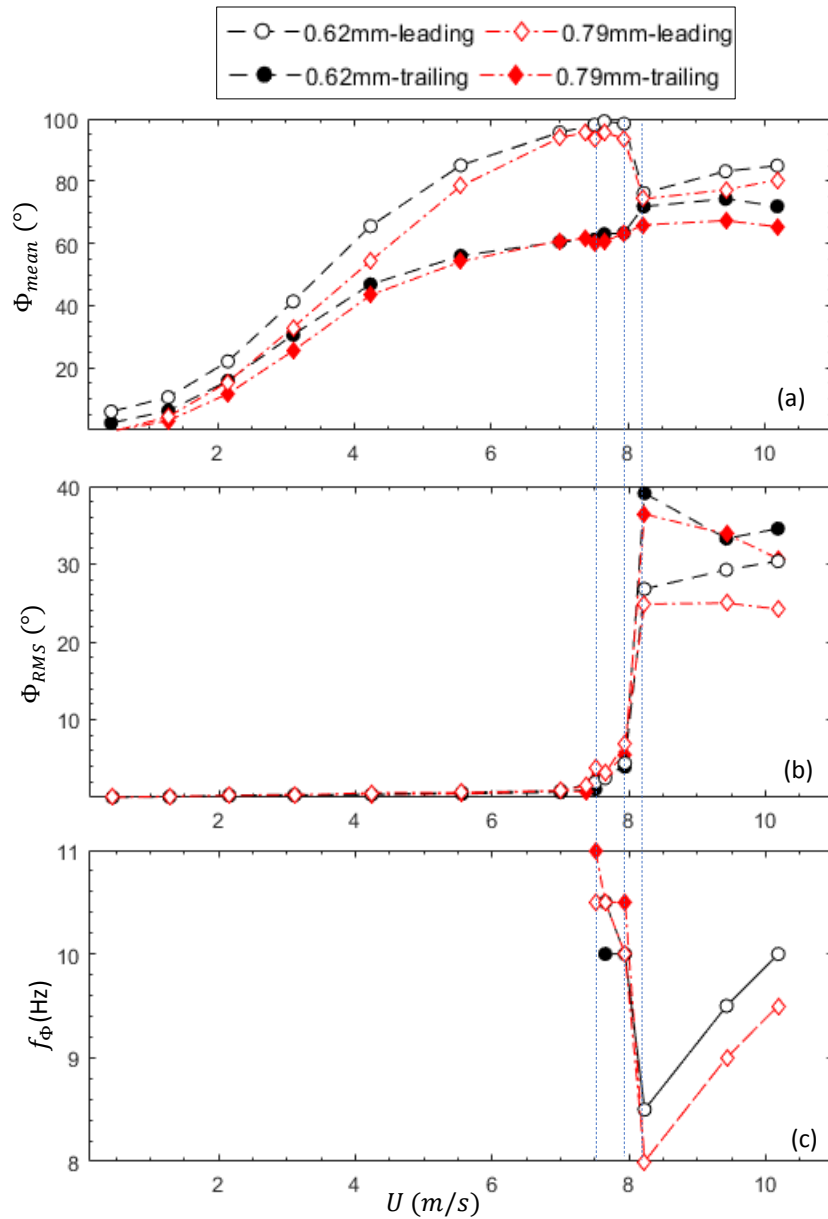


**Fig. 11.** Banner motion with the increase of flow speed at  $\theta_Y = 45^\circ$ . (a), (b), and (c) plot the mean, RMS, and frequency of  $\Phi$ , respectively, which describes the banner deflection, intensity, and frequency, respectively.

All the raw data in Fig. 6 and 9 are listed Table 2-5 in the Appendix.

## V. FSI Simulation models

The computational modeling data presented here is preliminary and limited to 2D modeling for now. We use a Cartesian grid, immersed boundary code (ViCar3D) to perform these simulations[16]. The simulations employ a diffuse interface, penalty immersed boundary method [16] for modeling the flow-induced flutter and further details regarding the numerical method can be found in Refs. [6, 16]. The simulations are conducted in a large  $(10l \times 10l)$  computational domain with a fine  $(576 \times 576)$ , non-uniform Cartesian grid. The Reynolds number for these simulations is 400, which is about one order of magnitude lower than the lowest Reynolds number in the experiment. However, as has been observed in the past [16], the flutter phenomena is relatively insensitive to the Reynolds number for  $Re > O(1000)$ .

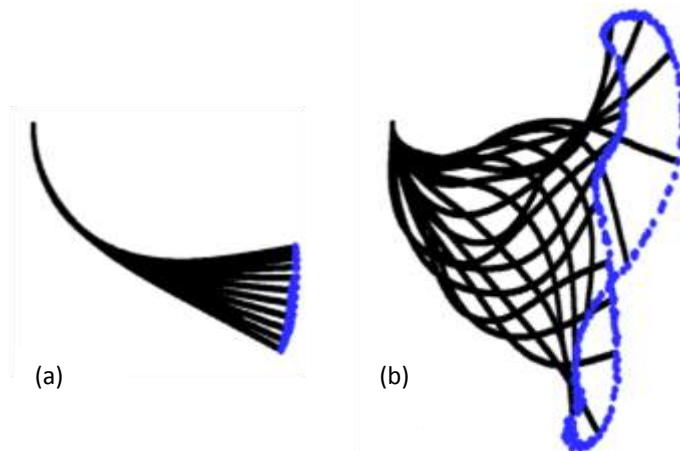


**Fig. 12. Simulation results showing motion envelope of the banner for two chosen behavior regimes: (a) small amplitude and (b) large amplitude flutter.**

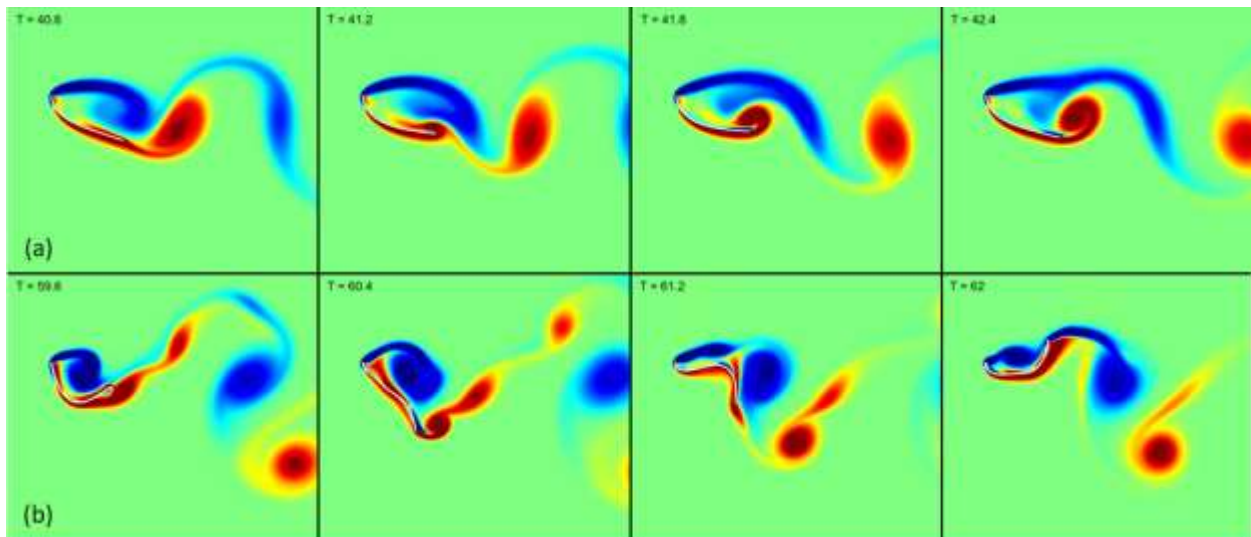


**Fig. 13. Vorticity snapshots for the two flutter behaviors for one cycle of each behavior.**

Figure 12 shows the motion envelope and the flutter dynamics for a banner at two different values of bending stiffness. Figure 13 shows vorticity snapshots for the two cases. The top set of snapshots shows low amplitude flutter behavior and here we can see that vortex shedding is similar to that for flow over an airfoil or flat plate at a medium angle-of-attack. The vortex shedding near the trailing-edge generates the small amplitude flutter of the banner. The bottom set of snapshots shows the high amplitude flutter case for the lower membrane stiffness. Here we observe more

complex flutter and vortex dynamics, and the trajectory of the membrane is at least qualitatively similar to that observed in the experiments. These preliminary simulations show that the flutter phenomena is quite robust and occurs even in 2D configurations at  $O(100)$  Reynolds numbers. Ongoing simulations will explore the parameter space and quantitative validation against experiments.

## VI. Conclusion

Flow-induced flutter of a hanging banner made of an elastic membrane is proposed as a benchmark for validation of computational models. Data from initial experiments for this configuration are presented. Using a high-speed imaging system, the deflection angle, flutter intensity and flutter frequency these hanging banners are investigated over a large range of flow velocities and two distinct yaw angles. A variety of distinct bifurcations and flutter regimes are found for these banners and this suggests that this configuration could indeed be useful for validation of computational models of flow-induced flutter. Results from preliminary 2D simulations at lower Reynolds numbers are also presented. The experiments and simulations for this configuration are ongoing and more detailed data will be presented in the future.

## Appendix

**Table 2: Experimental raw data for 0.62 mm banner at  $\theta_Y = 0^\circ$**

$U$ (m/s)	0.4	1.3	2.2	3.1	4.2	5.6	5.7	5.8	7.0	8.7	10.2	12.1	13.7	15.3	16.9
$\Phi_{mean}$ ( $^\circ$ )	3.6	8.8	19.6	35.0	48.4	60.7	59.4	68.6	74.8	70.9	70.9	72.3	70.9	71.8	72.0
$\Phi_{RMS}$ ( $^\circ$ )	0.0	0.2	0.5	0.6	0.5	0.6	0.5	15.5	21.9	28.9	35.4	35.3	33.9	35.1	34.2
$f_\Phi$ (Hz)	2.5	3.0	2.5	2.0	5.0	7.5	2.0	7.0	7.5	9.0	10.5	12.5	13.5	15.0	16.0

**Table 3: Experimental raw data for 0.79 mm banner at  $\theta_Y = 0^\circ$**

$U$ (m/s)	0.4	1.3	2.2	3.1	4.2	5.6	5.9	6.1	7.0	8.7	10.2	12.1	13.7	15.3	16.9
$\Phi_{mean}$ ( $^\circ$ )	6.5	9.8	18.1	30.6	43.4	53.4	57.5	62.1	72.0	74.3	69.8	70.2	66.3	70.0	72.3
$\Phi_{RMS}$ ( $^\circ$ )	0.0	0.1	0.5	0.6	0.8	0.5	0.8	11.4	16.4	22.8	31.4	34.3	33.9	35.0	36.3
$f_\Phi$ (Hz)	3.0	2.5	2.5	3.0	5.0	5.0	7.5	7.5	7.5	8.0	10.0	11.5	12.5	13.5	15.0

**Table 4: Experimental raw data for 0.62 mm banner at  $\theta_Y = 45^\circ$**

$U$ (m/s)		0.4	1.3	2.2	3.1	4.2	5.6	7.0	7.5	7.7	7.9	8.2	9.4	10.2
$\Phi_{mean}$ ( $^\circ$ )		5.9	10.6	22.1	41.3	65.5	85.0	95.6	98.1	99.2	98.4	76.1	83.2	85.0
$\Phi_{RMS}$ ( $^\circ$ )	Leading	0.0	0.1	0.3	0.3	0.4	0.6	0.9	1.9	2.5	4.4	26.8	29.3	30.4
$f_\Phi$ (Hz)		--	--	--	--	--	--	--	--	10.5	10.0	8.5	9.5	10.0
$\Phi_{mean}$ ( $^\circ$ )		2.3	6.2	15.9	30.6	46.8	56.0	60.5	61.2	63.0	63.3	71.8	74.3	71.9
$\Phi_{RMS}$ ( $^\circ$ )	Trailing	0.0	0.1	0.2	0.3	0.4	0.5	0.7	1.1	2.9	4.0	39.1	33.3	34.6
$f_\Phi$ (Hz)		--	--	--	--	--	--	--	--	10.0	10.0	8.5	9.5	10.0

**Table 5: Experimental raw data for 0.79 mm banner at  $\theta_Y = 45^\circ$  \***

$U$ (m/s)		0.4	1.3	2.2	3.1	4.2	5.6	7.0	7.4	7.5	7.7	7.9	8.2	9.4	10.2
$\Phi_{mean}$ ( $^\circ$ )		-0.6	4.3	15.4	33.0	54.3	78.4	93.9	95.5	93.8	95.7	93.6	74.3	77.2	80.4
$\Phi_{RMS}$ ( $^\circ$ )	Leading	0.0	0.1	0.3	0.3	0.6	0.6	0.9	1.5	3.9	3.1	7.0	24.9	25.0	24.2
$f_\Phi$ (Hz)		--	--	--	--	--	--	--	--	10.5	10.5	10.0	8.0	9.0	9.5
$\Phi_{mean}$ ( $^\circ$ )		-0.3	3.0	11.6	25.5	43.3	54.1	60.8	61.5	60.3	60.7	63.1	65.9	67.3	65.3
$\Phi_{RMS}$ ( $^\circ$ )	Trailing	0.0	0.1	0.3	0.4	0.4	0.5	0.8	0.7	2.4	3.1	5.5	36.4	33.9	30.7
$f_\Phi$ (Hz)		--	--	--	--	--	--	--	--	11.0	10.5	10.5	8.0	9.0	9.5

\* the negative value of  $\Phi_{mean}$  is due to measurement uncertainty.

## Acknowledgments

The authors thank Dr. Kourosh Shoele for discussions on flow-induced flutter. The computational method employed here has benefited from support from NSF grants IIS-1344772, CBET 1511200, TG-CTS100002 and AFOSR grant FA9550-16-1-0404.

## References

- [1] Slone, A.K., K. Pericleous, C. Bailey, M. Cross, and C. Bennett, A finite volume unstructured mesh approach to dynamic fluid-structure interaction: an assessment of the challenge of predicting the onset of flutter. *Applied Mathematical Modelling*, 2004. **28**(2): p. 211-239.
- [2] Zheng, L.X., T.L. Hedrick, and R. Mittal, A multi-fidelity modelling approach for evaluation and optimization of wing stroke aerodynamics in flapping flight. *Journal of Fluid Mechanics*, 2013. **721**: p. 118-154.
- [3] Zheng, L., T. Hedrick, and R. Mittal, A comparative study of the hovering efficiency of flapping and revolving wings. *Bioinspiration & Biomimetics*, 2013. **8**(3).
- [4] Mittal, R., B.D. Erath, and M.W. Plesniak, Fluid Dynamics of Human Phonation and Speech. *Annual Review of Fluid Mechanics*, Vol 45, 2013. **45**: p. 437-467.
- [5] Gilmanov, A. and S. Acharya, A computational strategy for simulating heat transfer and flow past deformable objects. *International Journal of Heat and Mass Transfer*, 2008. **51**(17-18): p. 4415-4426.
- [6] Shoele, K. and R. Mittal, Energy harvesting by flow-induced flutter in a simple model of an inverted piezoelectric flag. *Journal of Fluid Mechanics*, 2016. **790**: p. 582-606.
- [7] Hou, G., J. Wang, and A. Layton, Numerical methods for fluid-structure interaction—a review. *Communications in Computational Physics*, 2012. **12**(2): p. 337-377.
- [8] Holzinger, F., F. Wartzek, M. Jungst, H.P. Schiffer, and S. Leichtfuss, Self-Excited Blade Vibration Experimentally Investigated in Transonic Compressors: Rotating Instabilities and Flutter. *Journal of Turbomachinery-Transactions of the Asme*, 2016. **138**(4).
- [9] Tam, D., Flexibility increases lift for passive fluttering wings. *Journal of Fluid Mechanics*, 2015. **765**.
- [10] Hiroaki, K., M. Watanabe, and R. Morita, Flutter Analysis and Experiments of a Rectangular Sheet Supported by a Wire. *Proceedings of the Asme Pressure Vessels and Piping Conference - 2015, Vol 4*, 2015.
- [11] Boswirth, L., Theoretical and Experimental-Study on Valve Flutter .2. Flutter Experiments and Similarity. *Proceedings of the 1990 International Compressor Engineering Conference - at Purdue, Vols 1 and 2*, 1990: p. 684-698.
- [12] Zhang, J., S. Childress, A. Libchaber, and M. Shelley, Flexible filaments in a flowing soap film as a model for one-dimensional flags in a two-dimensional wind. *Nature*, 2000. **408**(6814): p. 835.
- [13] Turek, S. and J. Hron, Proposal for numerical benchmarking of fluid-structure interaction between an elastic object and laminar incompressible flow, in *Fluid-structure interaction*. 2006, Springer. p. 371-385.
- [14] Dou, Z., P.J. Ireland, A.D. Bragg, Z. Liang, L.R. Collins, and H. Meng, Particle-Pair Relative Velocity Measurement in High-Reynolds-Number Homogeneous and Isotropic Turbulence. *Experiments in Fluids*, 2017.
- [15] Adrian, R.J. and J. Westerweel, Particle image velocimetry. Vol. 30. 2010: Cambridge University Press.
- [16] Shoele, K. and R. Mittal, Computational study of flow-induced vibration of a reed in a channel and effect on convective heat transfer. *Physics of Fluids*, 2014. **26**(12).